Geometrical study of a hexagonal lattice photonic crystal fiber for efficient femtosecond laser grating inscription

Tigran Baghdasaryan,* Thomas Geernaert, Francis Berghmans, and Hugo Thienpont

Vrije Universiteit Brussel, Pleinlaan 2, 1050 Brussel, Belgium
**tbaghdas@b-phot.org*

Abstract: We have studied transverse propagation of femtosecond pulse duration laser light through the microstructure of hexagonal lattice photonic crystal fibers. Our results provide insight in the role of the microstructure on the amount of optical power that reaches the core of the PCF, which is of particular importance for grating inscription applications. We developed a dedicated approach based on commercial FDTD software and defined a figure of merit, the transverse coupling efficiency, to evaluate the coupling process. We analyzed the propagation of femtosecond laser pulses to the core of a wide range of PCFs and studied the influence of the PCF orientation angle, the air hole pitch and air hole radius on the energy reaching the core. We have found that the transverse coupling efficiency can benefit from a dedicated design of the microstructured cladding and an accurate fiber orientation. We designed a dedicated PCF microstructure that enhances transverse coupling to the core at a wavelength of 800 nm.

© 2011 Optical Society of America

OCIS codes: (060.2340) Fiber optics components; (060.5295) Photonic crystal fibers; (060.3735) Fiber Bragg gratings.

References and links

1. P. Russell, "Photonic crystal fibers," Science **299**(5605), 358–362 (2003).
2. J. M. Dudley, G. Genty, and S. Coen, "Supercontinuum generation in photonic crystal fiber," Rev. Mod. Phys. **78**(4), 1135–1184 (2006).
3. M. Napierała, T. Nasiłowski, E. Bereś-Pawlik, F. Berghmans, J. Wójcik, and H. Thienpont, "Extremely large-mode-area photonic crystal fibre with low bending loss," Opt. Express **18**(15), 15408–15418 (2010).
4. W. Wadsworth, R. Percival, G. Bouwmans, J. Knight, and P. Russell, "High power air-clad photonic crystal fibre laser," Opt. Express **11**(1), 48–53 (2003).
5. T. Martynkien, G. Statkiewicz-Barabach, J. Olszewski, J. Wojcik, P. Mergo, T. Geernaert, C. Sonnenfeld, A. Anuszkiewicz, M. K. Szczurowski, K. Tarnowski, M. Makara, K. Skorupski, J. Klimek, K. Poturaj, W. Urbanczyk, T. Nasilowski, F. Berghmans, and H. Thienpont, "Highly birefringent microstructured fibers with enhanced sensitivity to hydrostatic pressure," Opt. Express **18**(14), 15113–15121 (2010).
6. T. Geernaert, G. Luyckx, E. Voet, T. Nasilowski, K. Chah, M. Becker, H. Bartelt, W. Urbanczyk, J. Wojcik, W. De Waele, J. Degrieck, H. Terryn, F. Berghmans, and H. Thienpont, "Transversal load sensing with fiber Bragg gratings in microstructured optical fibers," IEEE Photon. Technol. Lett. **21**(1), 6–8 (2009).
7. G. Luyckx, E. Voet, T. Geernaert, K. Chah, T. Nasilowski, W. De Waele, W. Van Paepegem, M. Becker, H. Bartelt, W. Urbanczyk, J. Wojcik, J. Degrieck, F. Berghmans, and H. Thienpont, "Response of FBGs in microstructured and bow tie fibers embedded in laminated composite," IEEE Photon. Technol. Lett. **21**(18), 1290–1292 (2009).
8. X. Liu, X. Yang, F. Lu, J. Ng, X. Zhou, and C. Lu, "Stable and uniform dual-wavelength erbium-doped fiber laser based on fiber Bragg gratings and photonic crystal fiber," Opt. Express **13**(1), 142–147 (2005).
9. K. O. Hill and G. Meltz, "Fiber Bragg grating technology fundamentals and overview," J. Lightwave Technol. **15**(8), 1263–1276 (1997).
10. D. N. Nikogosyan, "Multi-photon high-excitation-energy approach to fibre grating inscription," Meas. Sci. Technol. **18**(1), R1–R29 (2007).
11. B. J. Eggleton, P. S. Westbrook, R. S. Windeler, S. Spälter, and T. A. Strasser, "Grating resonances in air-silica microstructured optical fibers," Opt. Lett. **24**(21), 1460–1462 (1999).
12. G. Kakarantzas, T. A. Birks, and P. S. Russell, "Structural long-period gratings in photonic crystal fibers," Opt. Lett. **27**(12), 1013–1015 (2002).
13. G. Brambilla, A. A. Fotiadi, S. A. Slattery, and D. N. Nikogosyan, "Two-photon photochemical long-period grating fabrication in pure-fused-silica photonic crystal fiber," Opt. Lett. **31**(18), 2675–2677 (2006).

#142371 - $15.00 USD Received 11 Feb 2011; revised 21 Mar 2011; accepted 21 Mar 2011; published 6 Apr 2011
(C) 2011 OSA

14. T. Geernaert, T. Nasilowski, K. Chah, M. Szpulak, J. Olszewski, G. Statkiewicz, J. Wojcik, K. Poturaj, W. Urbanczyk, M. Becker, M. Rothhardt, H. Bartelt, F. Berghmans, and H. Thienpont, "Fiber Bragg gratings in Germanium-doped highly birefringent microstructured optical fibers," IEEE Photon. Technol. Lett. **20**(8), 554–556 (2008).
15. Y. Wang, H. Bartelt, M. Becker, S. Brueckner, J. Bergmann, J. Kobelke, and M. Rothhardt, "Fiber Bragg grating inscription in pure-silica and Ge-doped photonic crystal fibers," Appl. Opt. **48**(11), 1963–1968 (2009).
16. C. Smelser, S. Mihailov, and D. Grobnic, "Formation of Type I-IR and Type II-IR gratings with an ultrafast IR laser and a phase mask," Opt. Express **13**(14), 5377–5386 (2005).
17. A. Martinez, M. Dubov, I. Khrushchev, and I. Bennion, "Direct writing of fibre Bragg gratings by femtosecond laser," Electron. Lett. **40**(19), 1170–1172 (2004).
18. G. D. Marshall, R. J. Williams, N. Jovanovic, M. J. Steel, and M. J. Withford, "Point-by-point written fiber-Bragg gratings and their application in complex grating designs," Opt. Express **18**(19), 19844–19859 (2010).
19. T. Geernaert, K. Kalli, C. Koutsides, M. Komodromos, T. Nasilowski, W. Urbanczyk, J. Wojcik, F. Berghmans, and H. Thienpont, "Point-by-point fiber Bragg grating inscription in free-standing step-index and photonic crystal fibers using near-IR femtosecond laser," Opt. Lett. **35**(10), 1647–1649 (2010).
20. J. Holdsworth, K. Cook, J. Canning, S. Bandyopadhyay, and M. Stevenson, "Rotationally variant grating writing in photonic crystal fibres," Open Opt. J. **3**(1), 19–23 (2009).
21. G. D. Marshall, D. J. Kan, A. A. Asatryan, L. C. Botten, and M. J. Withford, "Transverse coupling to the core of a photonic crystal fiber: the photo-inscription of gratings," Opt. Express **15**(12), 7876–7887 (2007).
22. J. Petrovic and T. Allsop, "Scattering of the laser writing beam in photonic crystal fibre," Opt. Laser Technol. **42**(7), 1172–1175 (2010).
23. S. Pissadakis, M. Livitziis, and G. Tsibidis, "Investigation of the Bragg grating recording in all-silica, standard and microstructured optical fibres using 248 nm, 5 ps laser radiation," J. Eur. Opt. Soc. Rapid Publ. **4**, 09049 (2009).
24. T. Geernaert, M. Becker, P. Mergo, T. Nasilowski, J. Wójcik, W. Urbańczyk, M. Rothhardt, C. Chojetzki, H. Bartelt, H. Terryn, F. Berghmans, and H. Thienpont, "Bragg Grating inscription in GeO_2-doped microstructured optical fibers," J. Lightwave Technol. **28**(10), 1459–1467 (2010).
25. J. Canning, N. Groothoff, K. Cook, C. Martelli, A. Pohl, J. Holdsworth, S. Bandyopadhyay, and M. Stevenson, "Gratings in structured optical fibres," Laser Chem. **2008**, 239417 (2008).
26. M. Becker, J. Bergmann, S. Brückner, M. Franke, E. Lindner, M. W. Rothhardt, and H. Bartelt, "Fiber Bragg grating inscription combining DUV sub-picosecond laser pulses and two-beam interferometry," Opt. Express **16**(23), 19169–19178 (2008).
27. S. J. Mihailov, D. Grobnic, H. Ding, C. W. Smelser, and J. Broeng, "Femtosecond IR laser fabrication of Bragg gratings in photonic crystal fibers and tapers," IEEE Photon. Technol. Lett. **18**(17), 1837–1839 (2006).

1. Introduction

Photonic Crystal Fibers (PCFs) were first proposed by Russell in 1991 [1]. The guiding properties of such fibers are essentially governed by the topology of air holes in the cross-section of the fiber cladding. This topology can be adapted to tailor the fiber properties for particular applications. PCFs are now used for different purposes in the field of photonics, e.g. supercontinuum generation [2], dispersion compensation [3], fiber lasers [4] and fiber sensors [5]. Fiber Bragg gratings and long period gratings are well-known essential elements in optical fiber technology. Many research efforts currently attempt to combine fiber gratings with the unique properties of PCFs for very diverse applications such as fiber sensing [5–7] and all-fiber lasers [8].

Grating inscription techniques for conventional step-index fibers have already been studied intensively in the last three decades [9,10]. They are now being revisited to allow efficient grating inscription in PCFs [11–15]. In most cases a UV laser and a phase mask are used, while the core of the fiber is often doped to increase its photosensitivity [9–15,24]. More advanced approaches rely on the use of high intensity laser radiation, where refractive index changes can even be induced in pure silica by a multi-photon absorption process [10,17–19,23]. Gratings inscribed by UV and IR femtosecond lasers have indeed been reported [10,13,16–19,27]. The main difficulty for multi-photon grating inscription in PCFs is the lattice of air holes in the cladding region that impedes the transverse propagation of light on its way to the core.

The first demonstration of a Bragg grating inscription in a PCF using a UV phase mask technique goes back to 1999 [11]. In this report the importance of the microstructured cladding configuration on the grating quality and its destructive effect on the amount of light reaching the core were first emphasized. Broader experimental studies relying on the UV inscription of gratings in GeO_2-doped PCFs with different air hole filling factors, air hole pitches and doping levels showed a moderate dependence of the reflection spectrum of the

#142371 - $15.00 USD Received 11 Feb 2011; revised 21 Mar 2011; accepted 21 Mar 2011; published 6 Apr 2011
(C) 2011 OSA

FBGs on the angular PCF orientation [20,24]. At the same time there are essential difficulties rising for the attempts to inscribe fiber Bragg gratings with 800 nm femtosecond lasers in pure silica PCFs. To the best of our knowledge 800 nm femtosecond gratings were only fabricated in few-holed and tapered PCFs [27].

Recently additional attention was paid to this issue by means of different simulation approaches. Ray tracing [20], semi-analytical multipole [21], finite element (FEM) [22] and finite difference time domain (FDTD) [20,23] methods were for example used to analyze the amount of optical power reaching the core. In all those reports a strong dependence of the angular PCF orientation was observed and a detrimental effect of the microstructured cladding was emphasized.

So far these simulations only considered commercially available PCFs with the ESM-12-01 fiber from NKT Photonics being chosen several times. These simulations did not exploit the design flexibility of a PCF and the resulting possibilities to optimize the microstructure to enhance transverse coupling to the fiber core.

In this paper we therefore optimize the geometrical parameters of a PCF to allow more efficient transverse coupling for femtosecond grating inscription mechanisms at 800 nm. We consider only PCFs with a hexagonal lattice of air holes as most PCFs feature that configuration. The air hole radius, air hole pitch and PCF orientation angle will be considered as variables and the influence on the laser pulse energy reaching the core will be investigated numerically.

Our paper is structured as follows. Section 2 describes the numerical model used and validates the simulation approach by comparing our results with literature data. In the same section the figure of merit for transverse coupling used throughout the paper is defined. Section 3 deals with the effect of the different parameters of a PCF on the transverse coupling efficiency. We also introduce a PCF with enhanced transverse coupling features at the end. We summarize our findings in and close our paper with section 4.

2. Numerical model and figure of merit for transverse coupling

The results in this paper are based on extensive numerical simulations relying on the Finite Difference Time Domain (FDTD) method. Previously used ray tracing methods proved not to be suitable for analyzing photonic crystal structures as the feature sizes of the geometry are comparable with the wavelength. FEM and multipole methods were successfully used to analyze PCFs. On the other hand FDTD is widely used for photonic crystal simulations [20,23] and a time domain evaluation of the pulse propagation through the microstructured cladding of the PCF can provide better understanding of the physical processes involved in the interaction of the laser pulse with the holey medium. For our FDTD calculations we used commercially available software from LUMERICAL running on a multi-processor computer with a large Random Access Memory (30GB).

In a first step we validate our approach by comparing our simulations with existing data from literature. We already mentioned that transverse light coupling to the core of PCFs was reported earlier; experimental and several numerical results are available in particular for the PCF ESM-12-01 [21–23]. These simulations mainly dealt with the dependence of the laser pulse energy reaching the core on the angular orientation of the fiber with respect to the impinging laser beams. Numerical simulations were performed both by multipole and FDTD methods giving similar results [21,23]. We have performed identical simulations of the transverse coupling dependence on the angular orientation of that PCF with our software. Our simulation geometry is illustrated in Fig. 1. The simulation area is surrounded by a Perfectly Matched Layer (PML) and the simulation time for every particular model is chosen to be long enough for the field to decay; typically below 1 ps.

Hexagonal lattice PCF has a 60° rotational symmetry in the microstructured cladding but we can even limit our investigation to angles between 0° and 30° due to the additional mirror symmetry. Here and throughout the paper 0° orientation corresponds to the ΓK direction of the hexagonal lattice. In the simulations we have used increments of 1° which is sufficient to obtain a clear picture of the angular dependence of the transverse coupling efficiency. Higher

#142371 - $15.00 USD Received 11 Feb 2011; revised 21 Mar 2011; accepted 21 Mar 2011; published 6 Apr 2011
(C) 2011 OSA

resolutions did not reveal additional angle dependent features. We used a frequency domain power monitor as detector in the simulations, the results of which were later extracted to MATLAB for post-processing. This procedure is illustrated in Fig. 1, which shows an example of the core field intensity distribution calculated by Lumerical FDTD with a rectangular detector covering the core region, together with the MATLAB processed data that represent the energy coupled to the core using a circular detector in the core area. The latter is found by introducing a circular detector with a specific radius that allows integrating the energy over the core region. The definition for the core region to be used throughout the paper will be presented further on in the section.

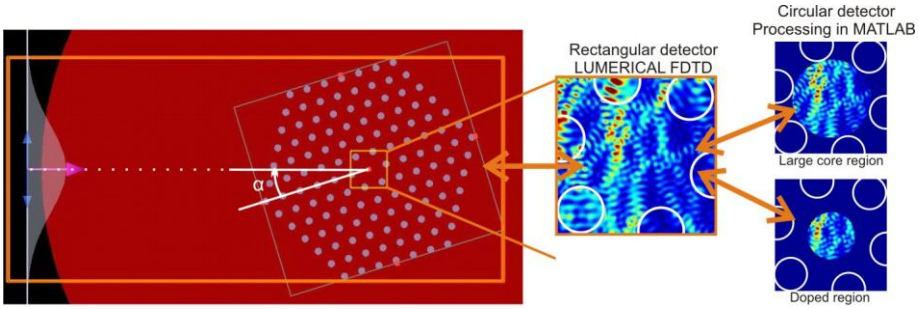

Fig. 1. Simulation geometry in LUMERICAL FDTD and MATLAB post-processed data.

Figure 2 depicts the results of our simulation for PCF ESM-12-01 with LUMERICAL FDTD, where every data point is calculated by integrating the intensity distribution over a circular frequency-domain detector region with a 12 μm diameter. The core field intensity for the PCF orientations from 0° to 30° relative to the incident beam is calculated for the 267 nm TE polarized 125 fs length incident pulse with a beam waist of 4 μm. We can state that the results of the simulations are in reasonable agreement with those of [21]; in particular we find the same angles equal to 56° and 64° that provide maximal transverse coupling. There are only slight differences which can be explained by the different simulation and post-processing approaches. Although the pulse length of the incident beam was not mentioned in [21], our simulations with 125 fs and 350 fs length pulses resulted in an identical dependence on the orientation angle. Good agreement of the results validates our approach and confirms that we can rely on our method to further analyze the influence of the PCF parameters on the transverse coupling efficiency.

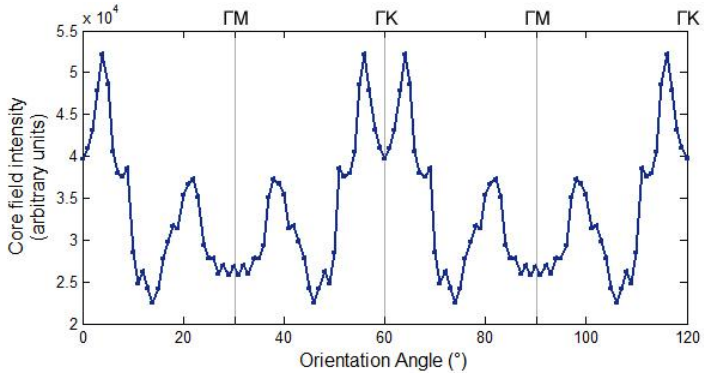

Fig. 2. Core field intensity dependence versus PCF ESM-12-01 orientation angle for transverse illumination with 125 fs length pulses at 267 nm.

Before doing so we first need to introduce a figure of merit that allows quantifying the amount of optical power effectively reaching the core of the PCF. Previous publications often only reported the intensity in arbitrary units, which compromises the understanding of the influence of the PCF cladding on the number of photons reaching the core. Only Pissadakis et

#142371 - $15.00 USD Received 11 Feb 2011; revised 21 Mar 2011; accepted 21 Mar 2011; published 6 Apr 2011
(C) 2011 OSA

al. [23] compared a standard step-index fiber with PCF ESM-12-01 for two angles to conclude on the detrimental influence of the microstructured cladding on the grating inscription. We therefore introduce the "Transverse Coupling Efficiency (TCE)" as a figure of merit for transverse coupling. This TCE is defined as the ratio of the core field intensity in the presence of a microstructured cladding to the core field intensity in absence of that same microstructured cladding. A TCE smaller than 1 indicates that the microstructured cladding has a detrimental influence on the delivery of the femtosecond pulse power to the core.

The TCE obviously depends on the radius of the circular core region that is used for the calculation of TCE. Since we study the TCE in the frame of grating inscription applications the overlap region between the mode area of the fundamental mode and the grating area should be considered. With femtosecond laser inscription, refractive index changes can be induced in both doped silica and pure silica. We therefore distinguish two types of fibers: when the PCF is doped (with GeO_2 for instance), the refractive index change is induced mainly in the photosensitive region. Hence the TCE calculation is based on a detection area with a radius that matches the doped region. In case of a non-photosensitive PCF the refractive index change can be induced in the entire fiber cross-section and therefore a larger core region (with a radius of air hole pitch minus air hole radius) should be considered. Core field intensity extraction for both of the cases is illustrated on the Fig. 1. Throughout the paper we presented all the data for those two models: doped PCF and non-photosensitive PCF models.

We consider a PCF with a 126 µm outer cladding diameter consisting of 6 rows of holes organized in a hexagonal lattice with an air hole pitch Λ of 3.46 µm and an air hole diameter d of 1.36 µm. The resulting filling factor is $d/\Lambda = 0.39$. The air hole pitch of this PCF is only half of that of the ESM-12-01 analyzed previously (see Fig. 3(a) and Fig. 3(b)). The smaller feature sizes of the PCF were chosen to be closer to the inscription wavelength (800 nm) which may result in a better TCE. For the TCE calculation it is also important to note that the radius of GeO_2-doped region in this particular PCF is 1.6 µm. The ratio of doped core radius to the entire core radius is 0.6; this ratio will be used for the TCE calculation in the doped PCF model. For the non-photosensitive PCF model a detector radius of Λ-*d/2* will be used.

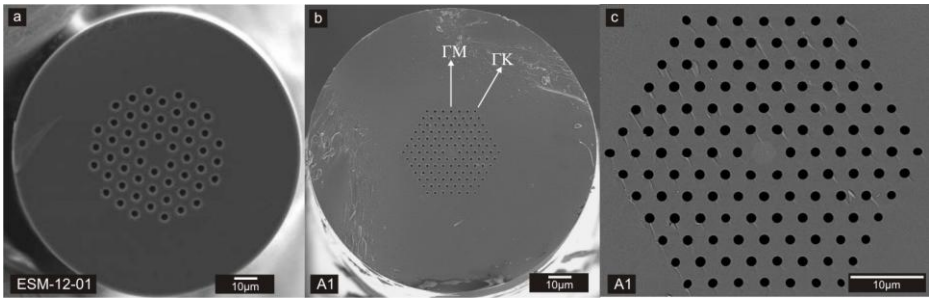

Fig. 3. SEM pictures of the ESM-12-01 and our PCF used as a model for simulations [24]. The doped region can be seen as a light gray region in the center of microstructure.

Another important issue to be considered when performing simulations is the influence of using as-built fiber cross-sections versus ideal cross-sections with perfectly circular holes and a perfect lattice. To check the influence of fabrication imperfections on the transverse coupling we have imported a scanning electron microscope image of the fabricated PCF (Fig. 3(c)) into LUMERICAL FDTD and performed the simulations on the TCE under the same conditions as for the ideal model. The results of the simulation on the ideal and as-built PCF are shown in Fig. 4. We find reasonable agreement between the two simulations with an average difference less than 9%. These results do not only validate our approach of using ideal structures, but also indicate the excellent manufacturing accuracy of this PCF.

#142371 - $15.00 USD Received 11 Feb 2011; revised 21 Mar 2011; accepted 21 Mar 2011; published 6 Apr 2011
(C) 2011 OSA

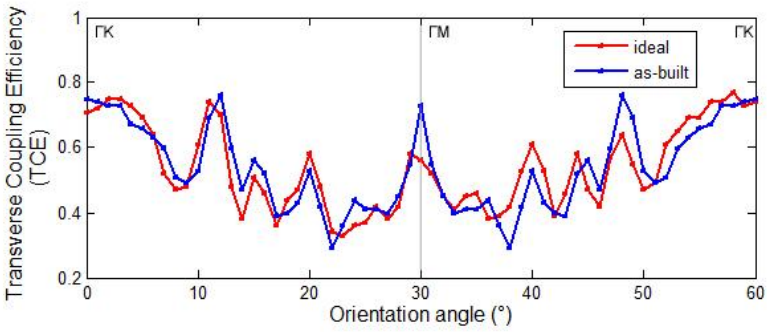

Fig. 4. Comparison of Transverse coupling efficiency (TCE) dependence on orientation angle for ideal and imported SEM A1 at 800 nm.

3. Transverse coupling efficiency (TCE) for IR 800 nm in hexagonal lattice PCFs

Ultrafast Ti:Sapphire lasers emitting at 800 nm are widely used for multi-photon grating inscription. These techniques often use lenses with relatively long focal distances (20-50 mm), hence with a low NA (less than 0.3) [14–16]. In contrast high NA lenses (up to 0.8) are used for point-by-point grating inscription [17–19]. For our 2-dimensional FDTD simulations we will use a femtosecond pulse of 125 fs at 800 nm with a Gaussian beam with a waist of 15 μm. We hereby attempt to mimic the configuration with a low NA lens, such as in a phase mask setup.

The goal of the investigation is to analyze the dependence of the PCF transverse coupling properties on the photonic crystal cladding parameters and to find a microstructured cladding configuration that favors grating inscription. We consider the following parameters of a hexagonal lattice PCF: the air hole radius (R), the air hole pitch (Λ) and the PCF orientation angle relative to incident beam (θ). Our approach is as follows.

1. We investigate 3 PCFs with different air hole radii under all possible orientation angles (θ), which allows drawing conclusions as to the orientation angles that yield the highest TCE and limiting further analyses to these angles.

2. We vary the air hole pitch (Λ) with the intention to further increase the TCE for the most favorable orientation angle found in step 1.

3. We study the influence of the air hole radius (R) for the PCF with the orientation angle and air hole pitch value that rendered the most favorable results after step 2.

All the results are presented for doped and non-photosensitive PCF models. The PCF geometry with the highest TCE value will then be analyzed in more details.

3.1. TCE dependence on PCF orientation angle

To investigate the influence of the orientation angle (θ) we considered 3 PCFs with a structure similar to the PCF shown in Figs. 3(b) and 3(c) and with different air hole radii (R): 0.68 μm, 1.1 μm and 1.5 μm. The air hole pitch is 3.64 μm yielding fill-factors (d/Λ) of 0.39, 0.64 and 0.87, i.e. low, average and high fill-factors. The simulations were performed for orientation angles from 0° to 30° with 1° increments and for TE polarized 125 fs pulses at 800 nm. Simulation of the pulse propagation through the PCF was performed in a region that covers the entire microstructure and part of the PCF's outer cladding (see Fig. 1).

The dependence of the TCE on the PCF orientation angle is shown in Fig. 5. A statistical analysis of the graphs is summarized in Table 1. The TCE clearly depends on the PCF orientation and there are obvious differences between the three types of PCFs. While the difference between the doped and non-photosensitive PCF models is purely quantitative; the position of the peak values and the overall angular dependence of the TCE are identical. A

#142371 - $15.00 USD Received 11 Feb 2011; revised 21 Mar 2011; accepted 21 Mar 2011; published 6 Apr 2011
(C) 2011 OSA

first and most significant result is that for the doped PCF model the TCE can be larger than 1 and it is observed at a 30° orientation in the high filling factor PCF. This implies that for this particular configuration the microstructured cladding has a beneficial effect on the amount of optical power that reaches the core for grating inscription, which is in contrast with literature that so far only reported on a detrimental influence of the microstructure on transverse coupling. This result also suggests that a dedicated PCF design and an accurate orientation of the fiber can enhance transverse power coupling to the core. The fact that the high filling factor PCF configuration exhibits the highest TCE is seemingly contra-intuitive since the presence of a microstructure in the cladding is more pronounced in this case.

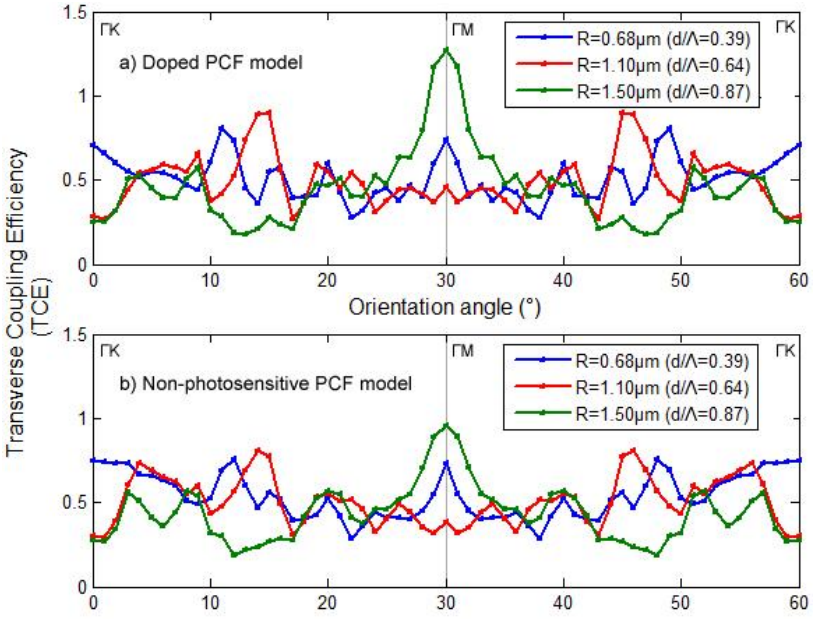

Fig. 5. Dependence of the Transverse Coupling Efficiency (TCE) on the orientation angle for the hexagonal lattice PCF with air hole pitch Λ of 3.46 μm and three values of air hole radius R at 800 nm. TCE calculations are done for a) doped and b) non-photosensitive PCF models.

For the non-photosensitive model, the TCE is always smaller than one. The latter observation together with the fact TCE higher than 1 is observed in case of smaller detector radius means that at 30° the energy is efficiently redistributed to the center of PCF.

Table 1. Statistical Data for Transverse Coupling Efficiency (TCE) Dependence on PCF Orientation Angle for Hexagonal Lattice PCF with Six Air Hole Rows

TCE	IR 800nm					
	Hole Radius					
	0.68 μm (d/Λ = 0.39)		*1.1 μm (d/Λ = 0.64)*		*1.5 μm (d/Λ = 0.87)*	
	Doped core	Large core	Doped core	Large core	Doped core	Large core
Mean TCE	0.51	0.54	0.49	0.51	0.45	0.44
Maximal TCE and corresponding PCF orientation angle	0.81 at 11°	0.76 at 12°	0.90 at 15°	0.81 at 14°	1.27 at 30°	0.96 at 30°
Minimal TCE	0.28	0.29	0.27	0.29	0.18	0.19
Standard deviation	0.126	0.134	0.157	0.144	0.229	0.169

Simulations for PCFs with 5 and 7 air hole rows (not presented here) confirmed the findings above; i.e. a peak value for the TCE was observed for the microstructures with a high filling factor (R = 1.5 μm, d/Λ = 0.87) at a 30° orientation. The simulations therefore lead to the first conclusion that the transverse coupling is most beneficial for a high filling factor PCF

#142371 - $15.00 USD Received 11 Feb 2011; revised 21 Mar 2011; accepted 21 Mar 2011; published 6 Apr 2011
(C) 2011 OSA

at a 30° orientation angle. Peculiar transverse coupling properties at 30° orientation were already reported in [25] where a high intensity in the PCF core was observed at that orientation angle. This particular feature for that angle can be understood from symmetry considerations: the structure is symmetric with respect to the propagation direction of the laser beam.

3.2. TCE dependence on PCF air hole pitch for 30° (ΓM) orientation

In this section we will further investigate the TCE dependence on the air hole pitch for a fixed value of the orientation angle (30°) and for two values of the air hole filling factor. The simulations were performed for two fixed values of d/Λ: 0.39 and 0.87. The first corresponds to the original A1 PCF, while the second was chosen in line with the results on the PCF orientation angle discussed in the previous section. The air hole pitch was varied from a value of 2 μm to 8 μm with increments of 0.1 μm; the lower limit of those values was chosen as a reasonable fabrication limit, while the upper limit corresponds to the air hole pitch of the ESM-12-01. The results of these simulations are presented in the Fig. 6.

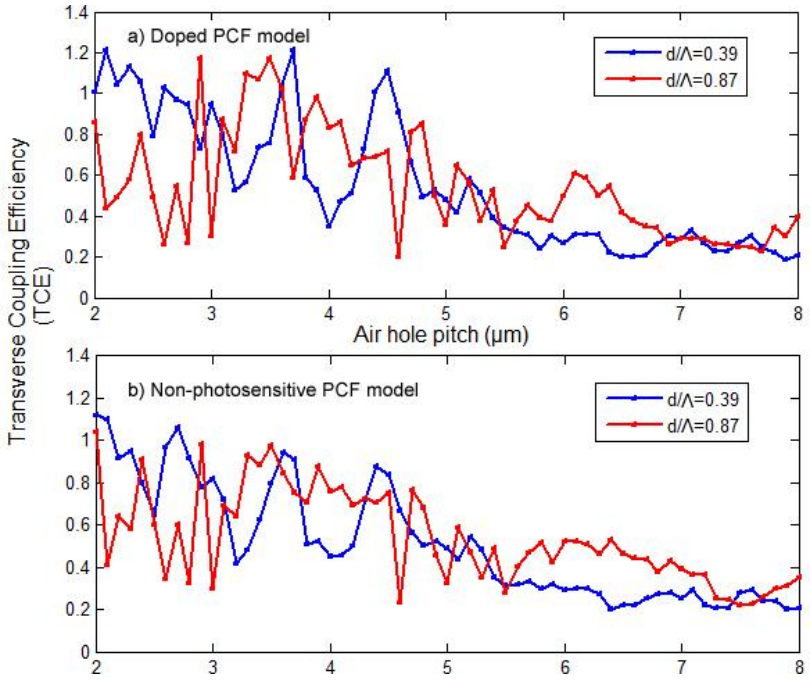

Fig. 6. Change of the TCE with the air hole pitch for the hexagonal lattice PCFs oriented at 30° for two different values of the filling factor at 800 nm. TCE calculations are done for a) doped and b) non-photosensitive PCF models.

The simulations as a function of the air hole pitch reveal the importance of this parameter for efficient grating inscription. The first significant result is that TCE values higher than 1 are mostly observed for the smaller values of the air hole pitch. It is important to note that in this case TCE higher 1 is observed not only for the doped PCF model, but for the non-photosensitive PCF model as well. Here we mention once more that the results for the two models are qualitatively identical. The simulation shows that for a laser wavelength of 800 nm the air hole pitch should not exceed ~5 μm to obtain high TCE values. We can conclude that the PCF air hole pitch should be sufficiently small to enhance efficient power delivery to the core. The low TCE values at air hole pitches exceeding 5 μm are in agreement with the detrimental influence of the microstructured cladding that was reported in literature [20–23].

#142371 - $15.00 USD Received 11 Feb 2011; revised 21 Mar 2011; accepted 21 Mar 2011; published 6 Apr 2011
(C) 2011 OSA

3.3. TCE dependence on PCF air hole radius for 30° (ΓM) orientation and optimized values of air hole pitch

The last parameter of the PCF to be optimized is the air hole radius. The orientation of the PCFs is at 30°, while the air hole pitch equals the values optimized in the previous section for two filling factors. The simulations of the TCE dependence on the air hole radius are carried out for PCFs with an air hole pitch of 3.46 μm and 3.7 μm. The range of possible air hole radii is limited by the air hole pitch: the hole radii will be varied from 0.6 μm to 1.7 μm for PCFs with a pitch of 3.46 μm; while for PCFs with pitch 3.7 μm air hole radii will be varied in a range of 0.6 μm to 1.8 μm.

From the results shown in Fig. 7 we conclude that there is a significant enhancement of the TCE for the PCF with Λ = 3.7 μm, when R = 1.64 μm. A TCE of 1.57 and 1.11, respectively for the doped PCF model and the non-photosensitive PCF model, are observed at that particular configuration. The filling factor for that optimal configuration is $d/\Lambda = 0.89$; which confirms that PCFs with a higher filling factor are more favorable for PCF inscription at 30°. At the same time high TCE values (higher than 1) are also observed for PCFs with other air hole radii and for PCFs with an air hole pitch of 3.46 μm. Finally TCE values larger than 1 can be observed for low filling factor PCFs as well which provides additional flexibility for the fiber design.

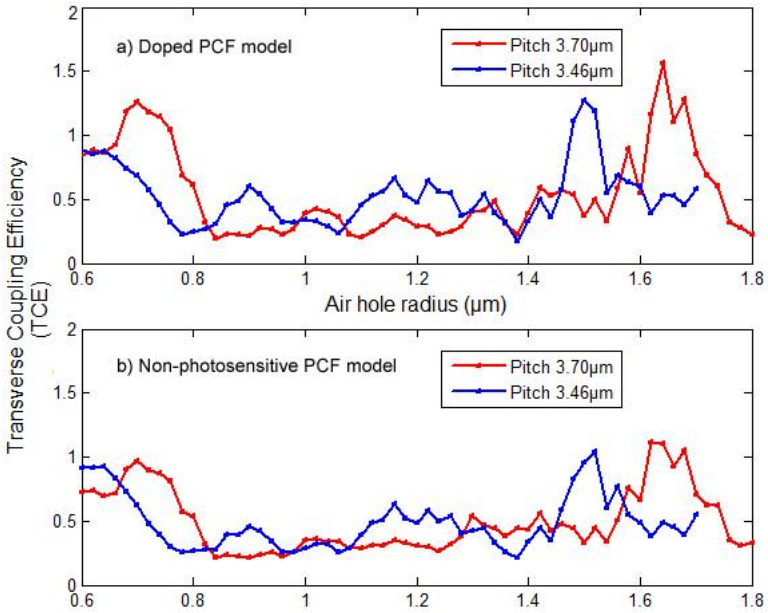

Fig. 7. Change of the TCE with the air hole radius for the hexagonal lattice PCFs at 30° (ΓM) orientation angle for two values of air hole pitch at 800 nm. TCE calculations are done for a) doped and b) non-photosensitive PCF models.

If we take a closer look at the TCE dependence on the air hole pitch, we can clearly see that high TCE values are observed in case of smaller values of Λ (Fig. 6). For the dependence on the air hole radius (Fig. 7) a high TCE is met for very low and very high air hole radii; in the first case the air hole dimensions and in the second case the width of the silica bridges (narrow silica regions in between of two air holes) are comparable with the wavelength. In Fig. 7 peaks of TCE dependence at high filling factor region for different air hole pitches are at R = 1.5 μm (for Λ = 3.46 μm) and at R = 1.64 μm (for Λ = 3.7 μm); simple calculations show that silica bridges are equal to 0.46 μm and 0.42 μm correspondingly; while the wavelength of the light is almost twice bigger (0.8 μm). The latter fact could mean that together with reflection and refraction effects, diffraction of light is also taking place during interaction of light pulse with air hole structure. All those results can bring to the conclusion

#142371 - $15.00 USD Received 11 Feb 2011; revised 21 Mar 2011; accepted 21 Mar 2011; published 6 Apr 2011
(C) 2011 OSA

that high TCE values observed in the paper result from resonance effects that stem from the dimensions of the PCF features which are comparable to the laser wavelength.

3.4. Analysis of the optimized PCF

In the previous sections we have found several efficient micro-structure configurations providing enhanced transverse coupling, i.e. TCE values exceeding 1. The investigation included the analysis of the dependence of the TCE on the orientation angle, the air hole pitch and the air hole radius. All the data were presented for two PCF models: one for doped and one for non-photosensitive cores. In the first case the radius of the circular detector for the TCE calculations was chosen to be comparable with a typical PCF doped area, while a larger detector radius was used in the second case (with radius of air hole pitch minus air hole radius). The best transverse coupling properties for a 125 fs pulse at 800 nm were obtained for an air hole pitch of 3.7 μm and air hole radius of 1.64 μm (d/Λ is 0.89) at 30°.

This PCF is shown in Fig. 8 together with the intensity distribution in the core for different orientation angles. For 30° orientation one can notice the high intensity region at the edge of the core region. The high peak intensity value at this focal point makes this particular PCF very attractive for multi-photon grating inscription, where a refractive index change is only taking place in regions with a sufficiently high optical intensity. The simulations at other orientation angles reveal a lower degree of transverse coupling in comparison with 30° incidence.

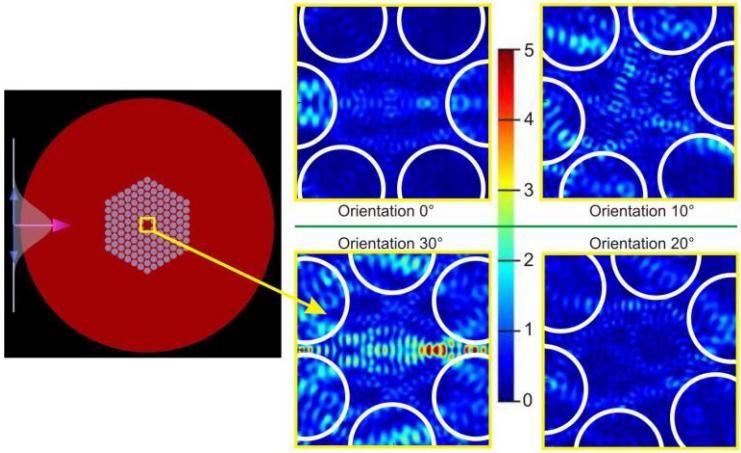

Fig. 8. Illustration of optimized PCF with Gaussian beam and corresponding normalized intensity distribution in the core part when illuminated by 125 fs pulse at 800 nm.

To gain even better understanding of the pulse propagation through the microstructured cladding we have also included a movie of the propagation of a 125 fs pulse through this PCF oriented at 30°. A still of the movie is shown in Fig. 9 (Media 1) to illustrate the intensity distribution of the femtosecond pulse as it reaches the PCF's core region. To some extent it illustrates how the pulse is 'guided' towards the center of the PCF as a result of a series of interactions with the 3 middle horizontal rows of air holes in the microstructure.

#142371 - $15.00 USD Received 11 Feb 2011; revised 21 Mar 2011; accepted 21 Mar 2011; published 6 Apr 2011
(C) 2011 OSA

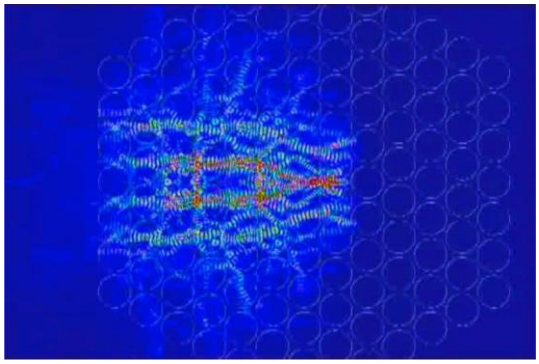

Fig. 9. Still from a movie illustrating 125 fs Gaussian beam propagation through the optimized PCF at 800 nm (Media 1).

From the animation and even from a still in Fig. 9 we can indeed hint at a physical explanation for the mechanism that causes the high TCE value in this PCF. After reaching the first air hole row, the electromagnetic field propagates mainly through the silica bridges (in between the air holes) between the middle horizontal row and the rows directly above and below. The 'guided' field hits the second air hole at the bottom of the air/silica interface and propagates through the holes. As a result of this scheme we observe light guiding through the photonic crystal structure by several 'waveguiding regions' until it reaches the core of the PCF. The latter can be considered as a defect in the photonic crystal structure, which allows two of those guided waves to interfere in the core region.

In general, transverse coupling to optical fibers for grating inscription applications is 3-dimensional. Here we have presented the reduced 2-dimensional (2D) problem. Our study can give a good starting point for further optimization in 3 dimensions. At the same time the results of the 2D simulations have a high degree of validity for long period grating inscriptions and even for grating inscription by two-beam interference method (e.g. in a Talbot interferometer), where typical values for the incidence angles are low enough (~15° and ~10° inside fiber) [15,26].

4. Conclusions

We have studied the transverse propagation of a femtosecond laser pulse to the core of a hexagonal lattice PCF for grating inscription purposes. Our approach relied on the assumption that the microstructured cladding of a PCF can be designed to allow more efficient grating writing. We considered multi-photon grating inscription with femtosecond pulses and a phase mask at a wavelength of 800 nm. Our model uses a 2D representation and an FDTD method. We introduced a figure of merit to allow interpreting the different results. This figure of merit was defined as a Transverse Coupling Efficiency (TCE) that corresponds to the ratio of the core field intensities in absence and in presence of the microstructured cladding. Photosensitive PCF with a central doped region and pure silica PCF were investigated in parallel throughout the paper.

First we have found that the microstructured PCF cladding does not necessarily have a detrimental effect on the inscription process. The microstructure, if well chosen, can indeed have a beneficial influence on the amount of optical power that reaches the PCF core. We have shown that in case of a dedicated design and under a controlled orientation of the PCF it is possible to gain advantage from the air hole microstructured cladding.

Second, we have found that the microstructure has a positive influence on the TCE for a higher filling factor when the PCF is oriented at the ΓM direction of the hexagonal lattice parallel to the beam propagation direction. TCE values in excess of 1 were also observed for other PCF configurations. Third, we observed an enhanced TCE for an air hole pitch smaller than 5 μm, indicating that in order to have enhanced transverse coupling the features of the microstructure should be sufficiently small.

#142371 - $15.00 USD Received 11 Feb 2011; revised 21 Mar 2011; accepted 21 Mar 2011; published 6 Apr 2011
(C) 2011 OSA

Finally, we described a PCF with an optimized design that returns a TCE of 1.57 and 1.11 for respectively the doped and pure silica PCF model at a 30° orientation. The intensity distribution in the core part of that PCF shows that the structure is focusing the incident beam to the edge of the core region, where the normalized intensity reaches very high values. This evidences that correctly designing a PCF may considerably impact effective multi-photon fiber Bragg grating inscription in these fibers.

Acknowledgments

The authors would like to acknowledge financial support from the European Commission Seventh Framework Programme project PHOSFOS, the COST TD1001 action, the Agency for Innovation by Science and Technology (IWT), the Research Foundation–Flanders (FWO), the Methusalem and Hercules Foundations Flanders, as well as the Interuniversity Attraction Poles (IAP)–Belgian Science Policy.

#142371 - $15.00 USD Received 11 Feb 2011; revised 21 Mar 2011; accepted 21 Mar 2011; published 6 Apr 2011
(C) 2011 OSA